Phase-field modeling of corrosion kinetics under dual-oxidants

2012 Modelling Simul. Mater. Sci. Eng. 20 035013

(http://iopscience.iop.org/0965-0393/20/3/035013)

Modelling Simul. Mater. Sci. Eng. **20** (2012) 035013 (12pp) doi:10.1088/0965-0393/20/3/035013

Phase-field modeling of corrosion kinetics under dual-oxidants

You-Hai Wen[1], **Long-Qing Chen**[2] **and Jeffrey A Hawk**[1]

[1] National Energy Technology Laboratory, Albany, OR 97321, USA
[2] Department of Materials Science and Engineering, Penn State University, University Park, PA 16802, USA

Received 26 May 2011, in final form 24 January 2012
Published 2 March 2012
Online at stacks.iop.org/MSMSE/20/035013

Abstract
A phase-field model is proposed to simulate corrosion kinetics under a dual-oxidant atmosphere. It will be demonstrated that the model can be applied to simulate corrosion kinetics under oxidation, sulfidation and simultaneous oxidation/sulfidation processes. Phase-dependent diffusivities are incorporated in a natural manner and allow more realistic modeling as the diffusivities usually differ by many orders of magnitude in different phases. Simple free energy models are then used for testing the model while calibrated free energy models can be implemented for quantitative modeling.

(Some figures may appear in colour only in the online journal)

1. Introduction

Advanced energy systems, such as oxyfuel and ultra-supercritical steam combustion boilers, oxyfuel and hydrogen turbines and advanced gasification systems, will operate at higher temperatures and in complex environments. Understanding how and being able to predict how materials perform in these complex environments is critical to enable these clean technologies to be brought on-line. Many of the components in these advanced applications will be exposed to a complex oxidizing environment. High corrosion rates under these environments make resistance to environmental attack an essential property for designers to include in life prediction calculations. To accelerate the development of these corrosion-resistant materials, it is highly beneficial to supplement the conventional experiment-based materials development program with a computational materials modeling approach to reduce the costs of materials development and implementation activities and to shorten the time for component insertion.

Due to the complexity of a typical multi-oxidant environment, it is very challenging if not impossible to predict the corrosion product with confidence. The computational approach available is largely based on thermodynamic calculations assuming thermodynamic equilibrium. For example, two-dimensional, isothermal stability diagrams are often used to assess the corrosion product of a metal exposed to a dual-oxidant atmosphere (figure 1). Unfortunately, there is usually a very large discrepancy between thermodynamically predicted

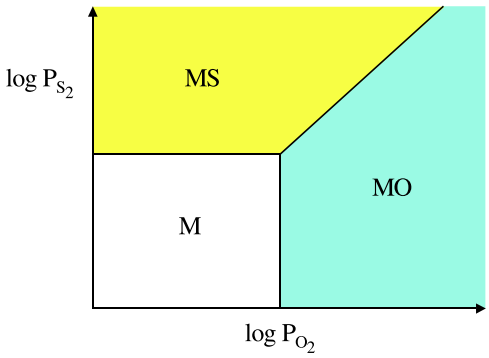

Figure 1. Schematic representation of a phase-stability diagram for a metal and its oxide and sulfide. (courtesy of Brian Gleeson).

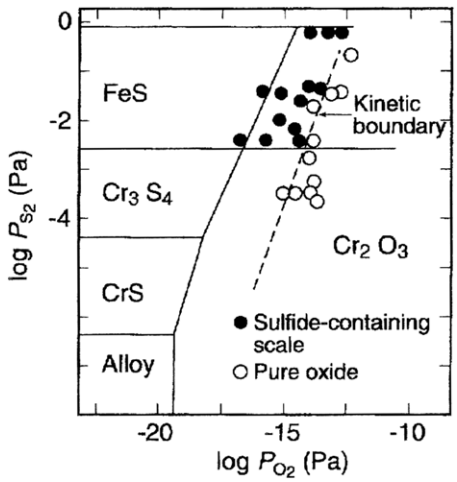

Figure 2. Thermodynamic phase-stability diagram for type 310 stainless steel at 875 °C with the experimentally determined kinetic boundary [1].

phase boundaries and experimentally observed ones. One such example is the corrosion of 310 type stainless steel exposed to dual-oxidants of oxygen and sulfur at 875 °C, as shown in figure 2 [1]. The actual P_{O_2} values for the transition from chromium-sulfide to chromium-oxide formation are about three orders of magnitude higher than the equilibrium values from thermodynamic calculations. The origin of this discrepancy is mainly due to kinetic effect such as significantly higher sulfidation rate than oxidation rate (generally 10^4–10^6 times higher for most metals due primarily to higher degree of non-stoichiometry in sulfides than in oxides), surface finish (adsorption of oxidants and nucleation kinetics of oxides/sulfides), etc. Also the stability diagrams usually do not have mixtures of oxides and sulfide that are frequently observed in experiments due to kinetic effect [2]. This indicates that a computational materials modeling approach that takes into account both thermodynamics and kinetics could potentially lead to more realistic predictions. The phase-field methodology is quite suitable as these are taken into account simultaneously. It has the potential to capture some transient states such as a mixture of oxides and sulfides.

In this work, a phase-field approach is proposed to simulate corrosion kinetics under a dual-oxidant atmosphere. This is an extension of a recent work where a phase-field approach was proposed to simulate oxidation kinetics under a single oxidant (Chen L Q, Wen Y H and Nafajabadi R 2011, unpublished). While the model formulation is generic with respect to any dual-oxidants, the two oxidants in this simulation are labeled as oxygen and sulfur for the sake of model description. In the following section, model formulation is described in detail, and a number of tests are carried out using phenomenological free energy models to demonstrate that the model can be used to simulate oxidation, sulfidation and simultaneous oxidation/sulfidation processes under various compositions of the two oxidants.

2. The phase-field model

For the description of the model, the two oxidants are labeled as oxygen (O_2) and sulfur (S_2). To simulate corrosion kinetics of a metal (M) exposed to a mixture of O_2 and S_2, the following chemical reactions need to be considered:

$$\mathrm{M} + \tfrac{1}{2}\mathrm{O_2} \leftrightarrow \mathrm{MO} \tag{1a}$$

$$\mathrm{M} + \tfrac{1}{2}\mathrm{S_2} \leftrightarrow \mathrm{MS} \tag{1b}$$

$$\mathrm{MO} + \tfrac{1}{2}\mathrm{S_2} \leftrightarrow \mathrm{MS} + \tfrac{1}{2}\mathrm{O_2}. \tag{1c}$$

In a phase-field model, different microstructures are described by field variables or 'phase-field parameters' which are continuous functions in space ($\vec{r}$) and time (t) domains. In the present case, the microstructure consists of metal, oxide and sulfide (M, MO and MS). Two phase-field parameters, i.e. $\eta_1(\vec{r}, t)$ and $\eta_2(\vec{r}, t)$, are needed to represent the microstructural distribution at a given time t. η_1 is introduced to represent the local phase fraction of sulfide and η_2 the local fraction of metal. The O_2 and S_2 compositions in mole fractions (X_o and X_s, respectively) are other field variables that are needed to describe the dual-oxidant composition profiles in the three phases. The compositions are assumed to be effective values which can be affected by possible reactions but the detailed reactions are not considered. Assuming that the free energies in the oxide and sulfide are, respectively, $f_\mathrm{mo}(X_\mathrm{o}, X_\mathrm{s})$ and $f_\mathrm{ms}(X_\mathrm{o}, X_\mathrm{s})$, following the work by Wang *et al* [3], the local free energy density of an oxide and sulfide two-phase zone can be expressed as

$$f^\mathrm{o}(\eta_1, X_\mathrm{o}, X_\mathrm{s}) = h(\eta_1) f_\mathrm{ms}(X_\mathrm{o}, X_\mathrm{s}) + (1 - h(\eta_1)) f_\mathrm{mo}(X_\mathrm{o}, X_\mathrm{s}) + w_1 g(\eta_1) \tag{2}$$

with

$$h(\eta_1) = \eta_1^3(6\eta_1^2 - 15\eta_1 + 10) \tag{3}$$

where (3) is a shape function and g(η_1) is a double-well potential given by

$$g(\eta_1) = \eta_1^2(1 - \eta_1)^2. \tag{4}$$

w_1 is the height of the imposed double-well free energy hump that describes the energy barrier for transformation between oxide and sulfide. The value of this quantity, along with the gradient energy coefficients shown below in equation (6), can be determined from interfacial energy and interface width.

Assuming that the free energy in the metal is $f_\mathrm{m}(X_\mathrm{o}, X_\mathrm{s})$, the local free energy density of an oxide, sulfide and metal system can be expressed as

$$f(\eta_1, \eta_2, X_\mathrm{o}, X_\mathrm{s}) = h(\eta_2) f_\mathrm{m}(X_\mathrm{o}, X_\mathrm{s}) + [1 - h(\eta_2)] f^\mathrm{o}(\eta_1, X_\mathrm{o}, X_\mathrm{s}) + w_2(\eta_1) g(\eta_2). \tag{5}$$

Note that the parameter w_2 is structure-dependent, i.e. $w_2 = w_2(\eta_1)$, to reflect the possible free energy barrier difference between metal/oxide and metal/sulfide.

The total free energy of an inhomogeneous system with oxide, sulfide and metal can be expressed as

$$F(\eta_1, \eta_2, X_o, X_s) = \int \left[f(\eta_1, \eta_2, X_o, X_s) + \sum_{i=1,2} \frac{\alpha_i}{2} (\nabla \eta_i)^2 + \sum_{i=o,s} \frac{\gamma_i}{2} (\nabla X_i)^2 \right] dV \tag{6}$$

where α and γ are the so-called gradient energy coefficients [4, 5]. The inclusion of these leading gradient energy terms in the total free energy accounts for their contribution to interfacial energy.

The temporal evolution of microstructure is governed by the time-dependent Allen–Cahn equation [5] for non-conserving phase-field parameters and the generalized Cahn–Hilliard equation [6] for conserving quantities on the basis of the phenomenological Fick–Onsager equations [7]:

$$\frac{\partial \eta_1(\vec{r}, t)}{\partial t} = -L_1 \frac{\delta F(\eta_1, \eta_2, X_o, X_s)}{\delta \eta_1} \tag{7a}$$

$$\frac{\partial \eta_2(\vec{r}, t)}{\partial t} = -L_2(\eta_1) \frac{\delta F(\eta_1, \eta_2, X_o, X_s)}{\delta \eta_2} \tag{7b}$$

$$\frac{\partial X_o(\vec{r}, t)}{\partial t} = \nabla \left[M_o(\eta_1, \eta_2) \nabla \frac{\delta F(\eta_1, \eta_2, X_o, X_s)}{\delta X_o} \right] \tag{7c}$$

$$\frac{\partial X_s(\vec{r}, t)}{\partial t} = \nabla \left[M_s(\eta_1, \eta_2) \nabla \frac{\delta F(\eta_1, \eta_2, X_o, X_s)}{\delta X_s} \right] \tag{7d}$$

where $\vec{r}$ and t represent spatial coordinates and time, respectively. L_1 and L_2 are the kinetic mobilities that describe the sulfidation rate from oxide and sulfidation/oxidation rate from metal, respectively. The structure-dependence of L_2, i.e. $L_2 = L_2(\eta_1)$, is used to describe the distinct kinetic rates of oxidation and sulfidation for the metal. M_i is the structure-dependent diffusion mobility of oxidant i. In this work, a linear interpolation is adopted to relate M_i with the mobilities of the oxidant in the metal (M_i^m), sulfide (M_i^{ms}) and oxide (M_i^{mo}). This is shown in equation (8):

$$M_i(\eta_1, \eta_2) = \eta_2 M_i^m + \eta_1(1 - \eta_2) M_i^{ms} + (1 - \eta_1)(1 - \eta_2) M_i^{mo}. \tag{8}$$

The ratio of the kinetic mobilities over the diffusion mobilities dictates whether the kinetic process (i.e. oxidation and sulfidation) is interface or diffusion limited. While the diffusion mobilities can be related to atomic mobilities [8], the kinetic mobilities are chosen in such a way that the kinetic process is diffusion controlled.

For this work, simple double-well free energy models are assumed:

$$\begin{aligned} f_m(X_o, X_s) &= \tfrac{1}{2}(X_o - X_m^o)^2 (X_s - X_m^s)^2 \\ f_{mo}(X_o, X_s) &= \tfrac{1}{2}(X_o - X_{mo}^o)^2 (X_s - X_{mo}^s)^2 \\ f_{ms}(X_o, X_s) &= \tfrac{1}{2}(X_o - X_{ms}^o)^2 (X_s - X_{ms}^s)^2 \end{aligned} \tag{9}$$

where X_p^q represents the equilibrium mole fractions of oxidant q in phase p for a temperature under consideration.

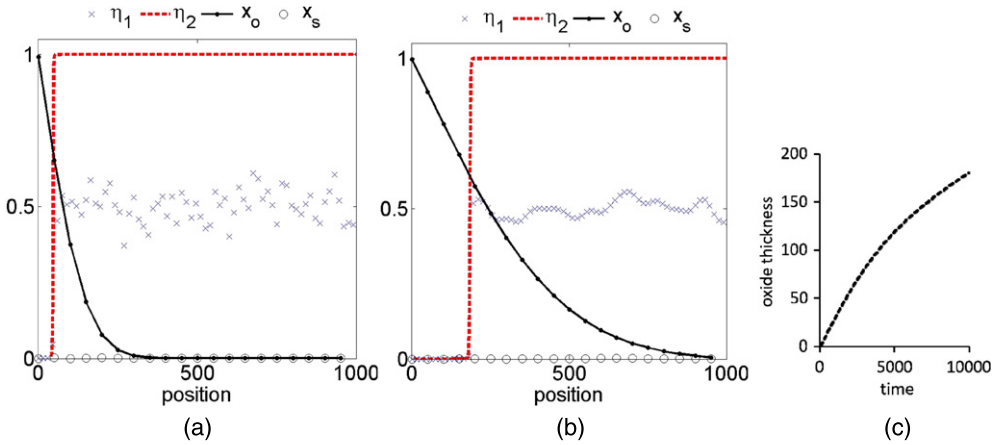

Figure 3. Phase-field parameters and composition profiles for oxidation modeling at three representative stages: (*a*) $t = 1000$; (*b*) $t = 10\,000$, and the corresponding oxidation kinetics (*c*).

3. Simulation results

This model is formulated to simulate corrosion kinetics of a metal exposed to a dual-oxidant atmosphere. Exposure of a metal to a single oxidant represents a simpler case. To evaluate the capability of this model to simulate corrosion kinetics under a single- or dual-oxidant condition, the metal is exposed to a single oxidant, e.g. oxygen or sulfur. This is followed by further testing where the metal is exposed to two oxidants. All calculations are carried out in one dimension (1D) with the following simplified model parameters (if not specified otherwise):

$$\alpha_1 = \alpha_2 = 10^{-5}, \quad w_1 = w_2(\eta_1) = 5 \times 10^{-3}, \quad X_{\mathrm{m}}^{\mathrm{o}} = X_{\mathrm{m}}^{\mathrm{s}} = 0.4, \quad X_{\mathrm{mo}}^{\mathrm{o}} = X_{\mathrm{ms}}^{\mathrm{s}} = 0.75,$$
$$X_{\mathrm{ms}}^{\mathrm{o}} = X_{\mathrm{mo}}^{\mathrm{s}} = 0.5,$$

$L_2(\eta_1)/L_1 = 1$, $\bar{M}/L = 2.5 \times 10^{-4}$, where $\bar{M}$ is a measure of mean diffusion mobility of the system,

$$M_{\mathrm{o}}^{\mathrm{m}}/\bar{M} = M_{\mathrm{o}}^{\mathrm{ms}}/\bar{M} = M_{\mathrm{o}}^{\mathrm{mo}}/\bar{M} = 1, \quad M_{\mathrm{s}}^{\mathrm{m}}/\bar{M} = M_{\mathrm{s}}^{\mathrm{ms}}/\bar{M} = M_{\mathrm{s}}^{\mathrm{mo}}/\bar{M} = 1,$$
$$\Delta x = 2.5 \times 10^{-2}, \quad \Delta t = 5 \times 10^{-4}.$$

3.1. Corrosion kinetics modeling under a single oxidant

3.1.1. Oxidation modeling. To simulate oxidation process of a metal under oxygen exposure, the composition of sulfur is set to zero in the bulk and at the two boundaries throughout the simulation. For oxygen composition, it is assumed to be zero in the bulk but a prescribed composition at the surface, which represents a dissolved oxygen composition from the surrounding atmosphere. The bulk is initially pure metal so η_2 is set to 1, but η_1 can be any value between 0 and 1, which is realized by assigning a randomly chosen value between 0 and 1 for each grid point. The nucleation of oxide is simulated by putting a nucleus at the surface and by setting η_1 and η_2 to 0.

Oxide grows with oxygen penetration from the surface into the bulk. As the oxide phase is described by a combination of $\eta_1 = 0$ and $\eta_2 = 0$, growth of oxide from a pure metal is characterized by a decrease in η_1 and η_2 to 0. Figure 3 shows the profiles of the phase-field parameters and compositions at three representative stages and the corresponding oxidation

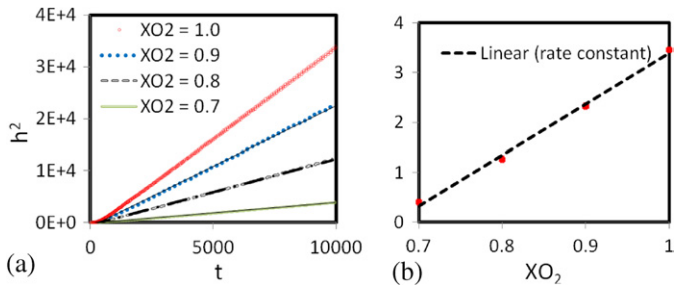

Figure 4. Effect of surface oxygen composition on oxidation kinetics (*a*) and the derived oxidation rate constants (*b*).

kinetics. Exposure of the metal to oxygen for 1k time steps leads to a visible oxide layer near the surface at the left of the computation domain (figure 3(*a*)). The thickness of the oxide can be measured by the distance between the surface and the oxide/metal interface. The oxide/metal interface coincides with the location where η_2 shows a step from 0 to 1. With further exposure to oxygen, this oxide layer keeps growing and the final profiles for this simulation are shown in figure 3(*b*) after 10k time steps.

The thickness of the oxide layer as a function of time is plotted in figure 3(*c*) showing a parabolic growth. This is in line with the experimental observation of oxidation kinetics at a high temperature. At a high temperature, the bulk diffusion is usually the dominant mechanism for oxygen transport. At a low temperature, however, the so-called short-circuit diffusion paths, such as grain boundaries and defects like voids, play a significant role in oxygen transport due to the relatively low diffusivity in the bulk. In the current 1D simulation, the effects of short-circuit diffusion paths have been ignored. Therefore, the simulated parabolic growth has only captured the high-temperature oxidation mechanism. To simulate low-temperature oxidation, the effect of microstructure such as grain structure (i.e. grain boundaries) and defect distribution (e.g. voids) needs to be considered, which can be readily taken into account in a higher dimensional model (2D/3D) that is beyond the scope of this work.

The parabolic rate constant, k_p, is dependent on the surrounding oxygen pressure as the defect chemistry such as oxygen vacancy concentration is a function of the partial pressure of oxygen (for a review see [9]). The dependence can usually be expressed as $k_\mathrm{p} \propto p_{\mathrm{O}_2}^n$ with parameter n in the range 1/6–1/4 [10, 11]. In this work, adsorption kinetics is not considered that relate the oxygen composition at the surface of the metal to the oxygen pressure in the surrounding environment. However, the effect of oxygen composition at the surface on oxidation kinetics can be considered by simply changing the boundary condition.

Figure 4 presents the simulated kinetics with various oxygen compositions at the surface. For the purpose of extracting the parabolic rate constants, the square of oxide thickness (h) is plotted versus the time (t) in figure 4(*a*) [12]. As can be seen, parabolic growth is observed in all these cases and the rate constant shows a linear dependence on the surface oxygen composition (figure 4(*b*)). To satisfy the relationship of $k \propto p_{\mathrm{O}_2}^n$, this linear dependence of the rate constant on surface oxygen composition suggests that the adsorbed oxygen should be related to the pressure of oxygen in the environment through $X_\mathrm{o}(x = 0) \propto p_{\mathrm{O}_2}^n$, which was proposed in the well-established Freundlich adsorption isotherm equation (Freundlich and Kuster 1894). This shows that the linear rate dependence shown in figure 4(*b*) is quite reasonable.

All the simulations so far have assumed identical oxygen diffusivities in the oxide and base metal. In reality, however, the diffusivities are usually drastically different from each other due to significantly different structures. The effect of varying diffusivity of base metal

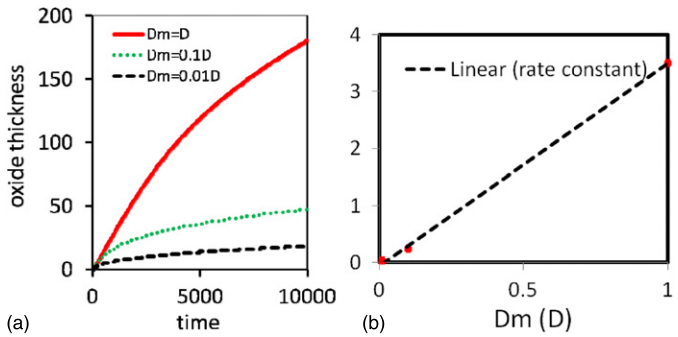

Figure 5. Effect of varying diffusivity of base metal on oxide thickness evolution (*a*) and the corresponding rate constants (*b*).

on the oxidation kinetics is shown in figure 5(*a*). The result in the solid line is the same result from figure 3(*c*). As the diffusivity in the metal is reduced by one (dotted line) and two orders (dashed line) of magnitudes, while keeping the diffusivity in the oxide unaltered, a decrease in the oxidation kinetics is observed as expected and the oxidation rate constant also decreases proportionally by one and two orders of magnitude, respectively.

3.1.2. Sulfidation modeling. The simulation set-up is similar to oxidation modeling except that the metal is now exposed to sulfur only, and a sulfide nucleus is introduced at the surface. Sulfide grows with sulfur penetration from the surface into the bulk. The results are very similar to those shown for oxidation modeling (figure 3). The only difference is the evolution of η_1. As the sulfide phase is represented by a combination of $\eta_1 = 1$ and $\eta_2 = 0$, growth of sulfide from a pure metal is accompanied by an increase in η_1 to 1 rather than a decrease to 0 as for oxide. The sulfidation kinetics is essentially identical to the oxidation kinetics. This is not surprising considering that identical diffusivities between oxide and sulfide are assumed as well as similar thermodynamics (free energy functional) between oxide and sulfide in these simulations.

3.2. Corrosion kinetics modeling under dual-oxidants

3.2.1. Oxidation under the influence of sulfur. The purpose of this section is to understand the effect of a relatively small amount of sulfur present in the environment on oxidation kinetics. The set-up is almost identical to that used for oxidation modeling. The only difference is that sulfur is present at the surface and it diffuses into the metal simultaneously with the oxygen. No sulfide nucleus is introduced at the surface.

Figure 6 shows the simulated kinetics under three different sulfur compositions at the surface of the metal with the baseline case represented by the solid line, as shown in figure 3(*c*). As can be seen, the presence of sulfur can significantly slow down the oxidation kinetics even without the formation of sulfide. The kinetic effect is ignored by assuming identical diffusivities for oxygen and sulfur in all phases, and the result is, therefore, a pure thermodynamic effect, i.e. composition dependence of free energies of oxide and metal phases that were adopted in the model.

3.2.2. Oxidation followed by sulfidation. In this simulation, the metal is first exposed to a pure oxygen environment with subsequent exposure to a sulfur only environment. An oxide

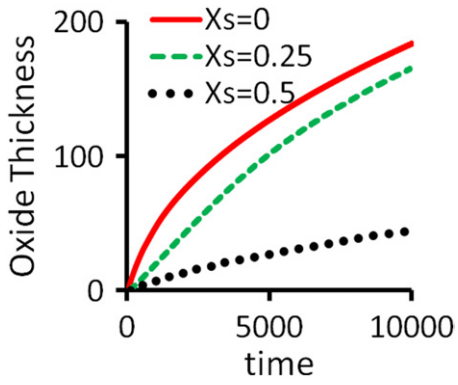

Figure 6. Effect of sulfur presence on oxidation kinetics.

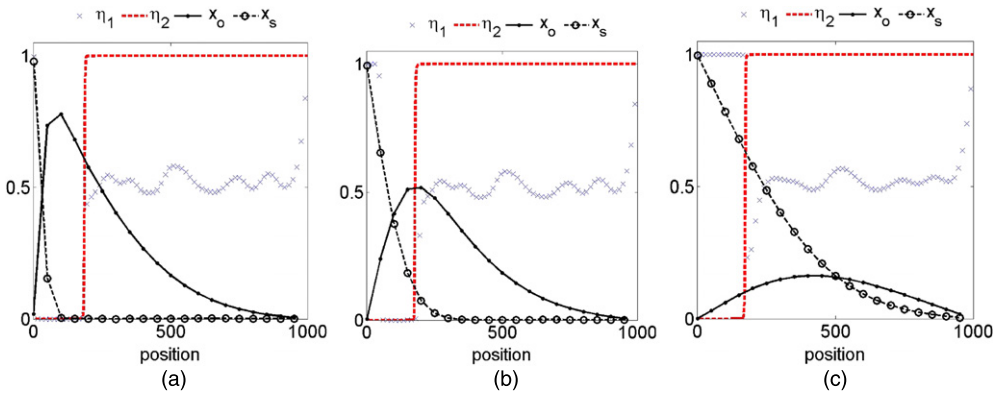

Figure 7. Phase-field parameters and composition profiles for oxidation and sulfidation modeling following a two-step exposure history: (*a*) shortly after the exposure transition to sulfur for 100 time steps after oxygen exposure until $t = 10\,000$; (*b*) after 1000 time steps of exposure to sulfur at $t = 11\,000$; (*c*) end of sulfur exposure at $t = 20\,000$.

nucleus is seeded at the surface at $t = 0$, and this is replaced by a sulfide nucleus at $t = 10\,000$ when sulfur begins to diffuse into the metal.

Figure 7 shows the evolution of phase-field parameters and composition profiles following the two-step exposure history. At the end of the exposure to oxygen at $t = 10\,000$, the phase-field parameters and composition profiles are those shown in figure 3(*b*). Immediately after this point, the metal is switched from oxygen exposure to sulfur exposure. Figure 7(*a*) is a snapshot of the profiles shortly after this transition reflecting the effect of reduced oxygen composition and increased sulfur composition at the surface. After some exposure to sulfur environment, as shown in figure 7(*b*), significant sulfur penetration is observed while oxygen leaves the system. As a result, significant sulfide is formed near the surface and oxide thickness shrinks from both ends with reduced oxygen composition. With further exposure to sulfur, the remaining oxide is eventually replaced by sulfide. Sulfide thickness keeps growing as seen at the final stage of the simulation in figure 7(*c*). The corresponding kinetics is shown in figure 8. Parabolic growth of oxide is followed by a gradual reduction in its thickness. It takes roughly 5000 time steps, which is approximately half of the oxygen exposure time, for the oxide to be completely removed. Parabolic growth is also found for sulfide growth although a small kink is observed at the point where oxide is totally removed.

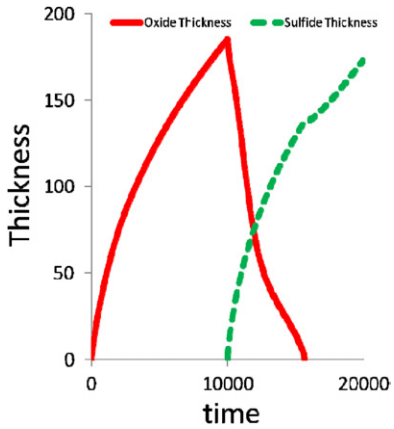

Figure 8. Oxidation and sulfidation kinetics under the two-step exposure history.

3.2.3. Simultaneous exposure to dual-oxidants. In this simulation, the metal is exposed to a mixture of relatively equal amount of the two oxidants. In this case, the kinetics plays a more important role in microstructure evolution. For example, nucleation kinetics of oxide/sulfide has a very strong effect on the final products. If an oxide (sulfide) nucleus exists at the surface, the oxide (sulfide) grows with continued supply of oxygen (sulfur) from the surface under the influence of the other oxidant. Provided that there are no other nucleation events, the final products would be determined by the surface nucleation itself. Further nucleation of oxide and sulfide is likely to occur, however, and the final products are, therefore, a dynamic balance of kinetics (i.e. nucleation kinetics in particular) and thermodynamics.

Nucleation modeling is beyond the scope of this work. An oxide nucleus is introduced at the surface, and no more nuclei are introduced in the simulation. To enhance dynamic effects, the diffusivities of sulfur (in the metal, oxide and sulfide) are set to be 10 times the value of those for oxygen diffusion. With this higher diffusivity for sulfur, its diffusion into the metal is faster. The current simulation explores the effect of sulfur in the environment, that is, whether enriched sulfur presence ahead of the growing oxide can trigger the nucleation of sulfide and affect the final products.

Figure 9 shows the snapshots of the phase-field parameters and composition profiles at a few selected representative stages. The initial stage is about the growth of the pre-existing oxide nucleus at the surface with the influx of both oxidants. The growth of the oxide is indicated by the reduction of η_1 and η_2 to 0 near the surface (albeit very thin and barely observable, as shown in figure 9(a)). Notice that the diffusion of sulfur is much ahead of oxygen. This has led to a sulfide nucleus formation right around this time with η_1 increased to 1 while maintaining the value of η_2 at 0 in a few grid points ahead of the oxide front. Continued exposure to the mixed oxidants leads to the growth of oxide and sulfide to quite an observable thickness, as shown in figure 9(b), where the oxide is located between the surface and the vertical blue (solid) line, and the sulfide between vertical blue (solid) line and the vertical red (dashed) line. Further exposure is accompanied by further growth of both oxide and sulfide and figure 9(c) corresponds to the final stage of the simulation. The combined kinetics plot shown in figure 9(d) indicates that sulfide grows at a relatively slower rate compared with that for oxide growth. This seems counter intuitive, that is, why does sulfide not grow faster with the much faster sulfur diffusion?

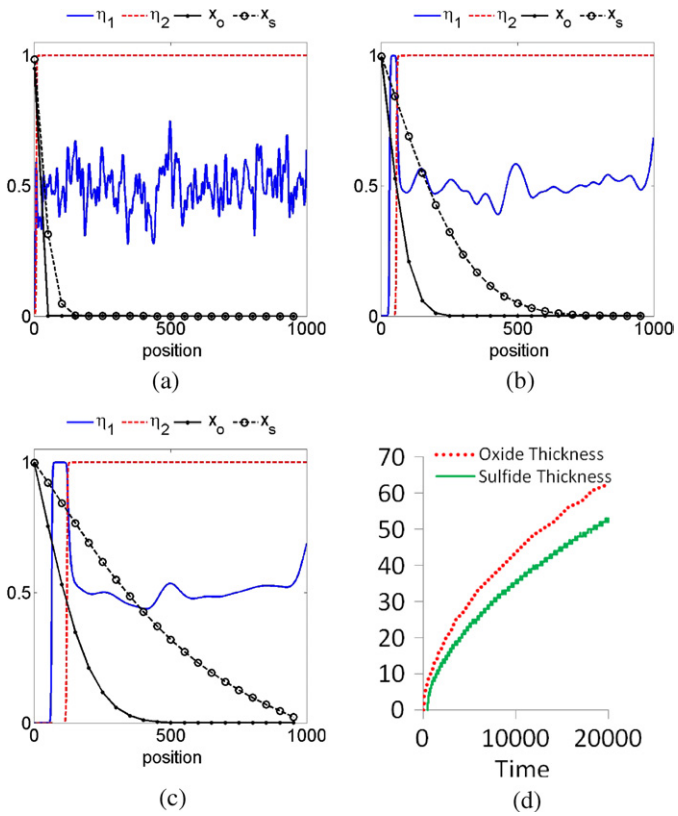

Figure 9. Selected phase-field parameters and composition profiles for simultaneous exposure to dual-oxidants: (*a*) $t = 200$; (*b*) $t = 5$k; (*c*) $t = 20$k; and the corresponding oxidation and sulfidation kinetics (*d*).

An examination of oxygen content at the sulfide/metal interface (the cross point between the η_2 profile and oxygen composition profile curves) reveals that there is approximately 0.45 oxygen at this point (figures 9(*b*) and (*c*)). Recalling how the presence of sulfide slows down the growth of oxide and that $X_s = 0.5$ has the most significant effect (figure 6), the same holds true here that the presence of significant oxygen content at the sulfide/metal interface acts as the limiting factor for the growth of sulfide (i.e. the sulfide/metal interface advancement). This exercise demonstrates that the kinetics in a dual-oxidant environment is much more complicated than a single-oxidant situation due to the coupled nature in the multi-oxidant case. In the current simulation, the diffusivities were assumed to be the same for oxygen and sulfur transport in all three phases (i.e. metal, oxide and sulfide) with faster sulfur diffusion. In reality, however, the diffusivities can be drastically different in the three phases. This will change the composition profiles of the two oxidants, and as a result the kinetics can be greatly affected.

4. Discussion

Oxidation kinetics of a metal is generally controlled by the diffusion process of the reactive species through the oxide layer and the base metal. The traditional approach to modeling

oxidation kinetics is to solve the classical Fick's diffusion equation. While analytical solution, e.g. error function solution (for a recent example see [13]), is limited to simple cases where the diffusivity is constant and boundary compositions are known, more realistic modeling needs to take into account the composition and microstructure dependent diffusion coefficients in the oxide layer and the moving boundary condition at the oxide/metal interface as well as complex geometries. A numerical method is generally considered the only option available for solving this problem.

A phase-field model was formulated to simulate corrosion kinetics for a metal in a dual-oxidant environment. The model can be used to simulate oxidation, sulfidation and simultaneous oxidation/sulfidation processes under various environments qualitatively. Phase-dependent diffusivities are incorporated in a natural manner, and as such, allows more realistic modeling as the diffusivities usually differ by many orders of magnitude in different phases. The present version of the model takes into account thermodynamic and kinetic effects explicitly. Thermodynamics for any particular system, which can usually be obtained through computational approach such as CALPHAD methodology, can be incorporated directly into the present formulation.

Simulations were carried out in 1D for the sake of testing the model. Implementation in higher dimension is needed to allow microstructure complexities, such as pores, grain structures and precipitates, in the metal to be introduced such that their effect on corrosion kinetics with the presence of so-called short-circuit diffusion paths can be assessed. In this work, only the inward diffusion of oxidants was considered while the effect of outward diffusion of metal was ignored. In addition, the oxidation reaction is not treated explicitly. All these should be considered for further development in order to develop a quantitative modeling tool for corrosion kinetics.

5. Summary

A phase-field model is proposed to simulate corrosion kinetics in dual-oxidant atmospheres. The model can be used to simulate corrosion kinetics under oxidation, sulfidation and simultaneous oxidation/sulfidation processes. Realistic free energy models and diffusivity data for various phases can be incorporated opening the door for quantitative modeling of corrosion kinetics. Work is in progress to include outward diffusion of metal and higher dimensional simulations incorporating microstructure complexities such as pores, oxide and alloy grain structures and precipitates.

Acknowledgments

The authors would like to thank David Alman, Brian Gleeson and Omer Dogan for helpful discussions, and Gordon Holcomb and the reviewers for carefully reading their manuscript and suggestions.

References

[1] Stroosnijder M F and Quadakkers W J 1986 *High Temp. Technol.* **4** 141
[2] Holcomb G 2011 private communication
[3] Wang S L, Sekerka R F, Wheeler A A, Murray B T, Coriell S R, Braun R J and McFadden G B 1993 *Physica* D **69** 189
[4] Cahn J W and Hilliard J E 1958 *J. Chem. Phys.* **28** 258

[5] Allen S M and Cahn J W 1979 *Acta Metall.* **27** 1085
[6] Cahn J W 1961 *Acta Metall.* **9** 795
[7] Kirkaldy J S and Young D J 1987 *Diffusion in the Condensed State* (London: Institute of Metals)
[8] Andersson J O and Ågren J 1992 *J. Appl. Phys.* **72** 1350
[9] Haugsrud R 2003 *Corros. Sci.* **45** 211
[10] Wagner C and Grunewald K Z 1938 *Phys. Chem.* B **24** 455
[11] Berry L and Paidassi J 1962 *C. R. Acad. Sci.* **255** 2253
[12] Pieraggi B 1987 *Oxid. Met.* **27** 177
[13] Li Y and Morral J E 2002 *Acta Mater.* **50** 3683